# Prediction of Adsorption of Nonionic Polymers from Aqueous Solutions to Solid Surfaces

**Sudip K. Pattanayek and Vinay A. Juvekar***

*Department of Chemical Engineering, Indian Institute of Technology Bombay, Powai, Mumbai 400 076, India*

*Received March 25, 2002; Revised Manuscript Received July 25, 2002*

ABSTRACT: In this paper, a model for predicting adsorption of nonionic polymers from aqueous solutions to solid surfaces has been presented. The model is based on continuum form of the self-consistent mean field theory. The model incorporates the effect of the hydrogen bond using Flory−Huggins model with a concentration-dependent Flory−Huggins parameter. The self-consistent field is derived using the Evans and Needham approach. The model has been validated using the reported experimental data on adsorption of poly(ethylene oxide) (PEO) from aqueous solution to silica. All the parameters of the model have been estimated from the reported data of the independent experiments specifically directed to obtain these parameters. Thus, the concentration-dependent Flory−Huggins parameter is estimated from the water activity in PEO solution, Kuhn length through the radius of gyration of PEO under Θ conditions, and polymer−surface affinity parameter through the specific enthalpy of displacement of water by PEO in the limit of zero adsorption. The model quantitatively predicts the adsorbed amount in trains, loops, and tails and the hydrodynamic thickness of the adsorbed layer. It also correctly predicts the effect of pH and molecular weight of PEO on these quantities. The advantage of this approach is that it allows direct extension of models, describing thermodynamics of hydrogen bond in the bulk, to the interfacial region. The other important contribution of this work is that it shows that, for estimation of the adsorbed amount in the form of trains, the calorimetric technique yields results which are consistent with the NMR spin relaxation technique.

## 1. Introduction

There exists a large class of nonionic water-soluble polymers. The industrially important polymers of this class include poly(ethylene oxide) (PEO) and its copolymers, polysaccharides, poly(vinylpyrrolidone), polyacrylamide, poly(vinyl alcohol), etc. Adsorption of these polymers on solid surfaces plays an important role in a variety of industrial applications. For example, adsorption of PEO is important in flocculation and hydrodynamic drag reduction.[1] High molecular weight PEO ($3 \times 10^6$) is used in mineral processing industry,[2] particularly for coal slurry dewatering.[3] Poly(vinylpyrrolidone) is used in cosmetics[1] and also for clarification of fruit juices, beer and in many other food processes.[4] Methyl derivatives of poly(vinyl ethers) are used in personal care applications.[1] Poly(vinyl alcohol) is used as protective colloid for emulsion polymerization of vinyl acetate[5] and vinyl chloride.[6] Polyacrylamide and starch are used in oil recovery applications.[3] Hydroxyl derivatives of poly(ethylene amine) are used as polymeric drug carriers.[1] The adsorption characteristics of all these polymers are significantly influenced by their ability to form hydrogen bonds among themselves, with water, and with the solid surface. Models for predicting the adsorption characteristics, as well as the extent to which the surface properties are modified after adsorption, should appropriately account for the effect of this hydrogen bonding. A number of models for predicting bulk thermodynamic properties of hydrogen bonding systems are available in the literature. These include the bond counting approach of Levine and Perram[7] and Veytsman,[8] reaction equilibrium models of Iconomou and Donohue,[9] Panayiotou,[10] and Panayiotou and Sanchez,[11,12] the integral equation theory of Cummings and Stell,[13] and the thermodynamic perturbation theory of Wertheim.[14] Out of these, only the model of Panayiotou and Sanchez[12] has been used to predict the thermodynamics of polymer solutions. Difficulty arises when one attempts to extend these models to the interfacial region. Here the entropy of hydrogen bonding is affected by the anisotropy of this region. A predictive model should correctly quantify this effect. This is a difficult task. Cummings and Stell's[13] theory and the density functional theory of Segura et al.[15] have been applied to small associating molecules near solid surfaces. Because of the inherent complexity of these models, extending them to describe the systems involving polymers is extremely difficult. Cohen Stuart et al.[16] have applied the lattice-based model of Scheutjens and Fleer[17] to predict the adsorption characteristics of PEO from water on polystyrene latex. However, no specific attempt has been made to account for the hydrogen bond effect. Although their model is able to correctly predict the trends of variation of the adsorbed amount and the hydrodynamic thickness of the adsorbed layer with the molecular weight of PEO, the theory has not been quantitatively tested against the experimental data. Only recently, Suresh and Naik[18−20] have developed a model which combines the bond counting approach[8] with the lattice-based self-consistent mean field theory of Scheutjens and Fleer.

An alternative approach to extend any bulk-interaction model to the interfacial region has been proposed by Evans and Needham[21] (also see the work of Ploehn[22]). In this technique, the interfacial region is viewed as a continuum. The chemical potential $\mu_i$ of the species $i$, at any location, $z$, in the interfacial region is written as the sum of a homogeneous and a nonhomogeneous component. The homogeneous component is computed

* To whom the correspondence should be addressed. Email: vaj@che.iitb.ac.in.

10.1021/ma020478i CCC: $22.00 
Published on Web 10/29/2002

using the local fluid composition at $z$, assuming that the fluid is spatially homogeneous. The nonhomogeneous component arises due to the anisotropy introduced by the connectivity of the polymer chain. The monomeric species have only the homogeneous component associated with them. The nonhomogeneous component of species $i$ is determined through constrained variational minimization of the free energy functional of the interfacial region with respect to the volume fraction profile of the species. The imposed constraints are those of the Gibbs−Duhem equation, constancy of the total volume, that the volume fractions sum up to unity at every location and any other constraints which are externally imposed. The self-consistent potential of the polymeric species is then obtained by subtracting the entropic contribution from the nonhomogeneous components of its chemical potential. This potential can be used in the self-consistent field calculations to arrive at the equilibrium composition of the interfacial region. The advantage of this procedure is that, to compute the self-consistent potentials, one only needs the chemical potentials of species in a spatially homogeneous solution. This allows direct extension of the thermodynamic models for the bulk solution to the interfacial region. Thus, the complication associated with the computation of hydrogen bond entropy in the interfacial region is avoided by this procedure.

In this work, we have combined the approach outlined above with the continuum version of the self-consistent field theory previously developed by us.[23] Although, any one of the various available bulk thermodynamics models can be used here, we have chosen the modified Flory−Huggins theory in which, to account for hydrogen bonding, the Flory−Huggins $\chi-$ parameter is expressed as a function of the volume fraction of the polymer. The use of concentration-dependent $\chi-$ parameter is not new. It has been previously employed for predicting the lower critical solution temperature (LCST) of both the non-hydrogen bonding (Quian et al.[24]) and hydrogen bonding (Bae et al.[25]) polymer systems. The advantage of the Flory−Huggins model lies in its simplicity and ease with which it can be fitted to the bulk solution data.

The PEO−water−silica system has been chosen as the test case for validating the theory, since, on this system, the literature provides adequate amount of the experimental data required for validating the model. We have used these data to quantitatively evaluate the predictions of the model. The parameters required for the model are obtained from the reported results of the independent experiments, which are specifically directed to obtain those parameters.

In the following text, we first describe the procedure for determining the concentration- and temperature-dependent $\chi-$ parameter for PEO−water system using the water-activity data reported in the literature. We then derive the expression for the self-consistent field in the interfacial region, in relation to the continuum model. Next we describe the procedure for estimating the model parameters. Finally, we validate the model by comparing the model predictions of various characteristics of the adsorbed layer, with the reported experimental data on those characteristics.

## 2. Correlation of the Bulk Thermodynamic Data for the PEO−Water System

According to the Flory−Huggins theory, the free energy of mixing of $n_p/r$ polymer chains, with each polymer chain consisting of $r$ segments, and $n_w$ moles of solvent (water) to form a solution containing $\phi_p$ volume fraction of the polymer and $\phi_w$ volume fraction of the solvent is given by

$$\frac{F}{kT} = n_w \ln(\phi_w) + \frac{n_p}{r}\ln(\phi_p) + \chi n_w \phi_p \tag{1}$$

Here, the amorphous polymer and pure water are used as the datum states. To account for hydrogen bond effect, we consider the Flory−Huggins interaction parameter, $\chi$, to be a function of $\phi_p$. Chemical potential of water molecule and PEO segment in a homogeneous solution can then be expressed as

$$\frac{\mu_w^h}{kT} = \left(\frac{\partial(F/kT)}{\partial n_w}\right)_{n_p} = \ln(\phi_w) + \phi_p\left(1 - \frac{v_w}{r v_p}\right) + \chi\phi_p^2 - \phi_w\phi_p^2\frac{\partial\chi}{\partial\phi_p} \tag{2}$$

$$\frac{\mu_p^h}{kT} = \left(\frac{\partial(F/kT)}{\partial n_p}\right)_{n_w} = \frac{1}{r}\ln(\phi_p) + \phi_w\left(\frac{1}{r} - \frac{v_p}{v_w}\right) + \chi\frac{v_p}{v_w}\phi_w^2 + \phi_w^2\phi_p\left(\frac{v_p}{v_w}\right)\frac{\partial\chi}{\partial\phi_p} \tag{3}$$

where $v_p$ and $v_w$ represent the partial molar volumes of the polymer segment and water, respectively.

From eq 2, we obtain the expression for the activity of water, $a_w$, in the aqueous PEO solution as

$$\ln a_w = \frac{\mu_w^h}{kT} = \ln\phi_w + \phi_p\left(1 - \frac{v_w}{r v_p}\right) + \chi\phi_p^2 - \phi_w\phi_p^2\frac{\partial\chi}{\partial\phi_p} \tag{4}$$

We define the quantity, $\beta_w$, as

$$\ln\beta_w = \ln a_w + \frac{v_w}{r v_p}\phi_p = \ln\phi_w + \phi_p + \chi\phi_p^2 - \phi_w\phi_p^2\frac{\partial\chi}{\partial\phi_p} \tag{5}$$

The quantity $\beta_w$ is independent of the chain length and hence different lengths of PEO chains follow a single curve relating $\beta_w$ to $\phi_p$ as shown in Figure 1. To correlate these data we express $\chi$ at constant temperature $T$, as a quadratic polynomial in $\phi_p$:

$$\chi = a(T) + b(T)\phi_p + c(T)\phi_p^2 \tag{6}$$

The least-squares fits are shown by lines in Figure 1. The percentage error for each of the fit from the actual data is also listed in the plot. The coefficients, $a(T)$, $b(T)$, and $c(T)$, obtained for each of the three temperatures are then correlated using a quadratic polynomial in $1/T$. These relations are listed in Table 1.

To check the accuracy of the above correlation, we use it to predict the low-pressure phase-separation data of PEO−water system. At the point of phase separation,

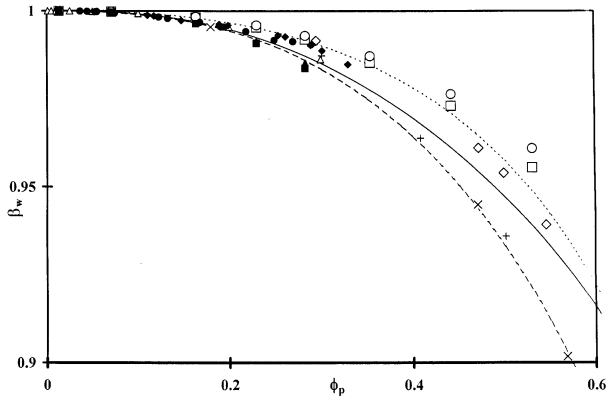


**Figure 1.** Activity of water in aqueous PEO solution at temperatures of 298 (—), 313 (— —), and 333 K (···). Experimental data points: (▲) Hasse et al.[26] [$M_p$ = 23 000, $T$ = 298 K]; (■) Hasse et al.[26] [$M_p$ = 35 000, $T$ = 298 K], (●) Haynes et al.[27] [$M_p$ = 3350, $T$ = 298 K]; (◆) Haynes et al.[27] [$M_p$ = 8000, $T$ = 298 K]; (△) Hasse et al.[26] [$M_p$ = 6000, $T$ = 313 K]; (×) Herskowltz and Gottlieb[28] [$M_p$ = 1500, $T$ = 313 K]; (+) Herskowltz and Gottlieb[28] [$M_p$ = 6000, $T$ = 313 K]; (□) Gaube et al.[29] [$M_p$ = 1500, $T$ = 333 K]; (◇) Herskowltz and Gottlieb[28] [$M_p$ = 6000, $T$ = 333 K]; (○) Gaube et al.[29] [$M_p$ = 3000, $T$ = 333 K]. Percent errors of the best fit curves from the experimental data are 0.2 at 298 K, 0.6 at 313 K, and 0.4 at 333 K.

**Table 1. Regression Estimates of Polynomials $a(T)$, $b(T)$, and $c(T)$ of Eq 6**

$$a(T) = 1.14807 - (43.437/T) + (770.88/T^2)$$
$$b(T) = 0.56642 - (33.928/T) + (596.07/T^2)$$
$$c(T) = 0.21712 - (8.6589/T) + (300.03/T^2)$$

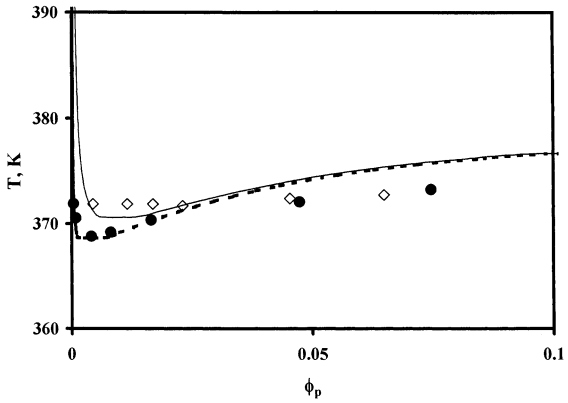


**Figure 2.** Phase equilibrium data for PEO−water solution: (◆) Saeki et al.[30] ($M_p$ = $10^6$); (●) Bailey and Callard[31] ($M_p$ = 7 × 106). Predicted data are shown by a solid line (—) and a dotted line (···), respectively.

we have $\partial\mu_p^h/\partial\phi_p = 0$, which, in view of eq 3, requires that

$$\frac{1}{\phi_p}\frac{v_s}{rv_p} + \frac{1}{(1-\phi_p)} - 2\chi + 2(1-2\phi_p)\frac{\partial\chi}{\partial\phi_p} + \phi_p(1-\phi_p)\frac{\partial^2\chi}{\partial\phi_p{}^2} = 0 \quad (7)$$

After substitution of $\chi$ from eq 6 into eq 7, a quartic equation in $\phi_p$ is obtained. At a given temperature and chain length, two real roots of this polynomial in the range of $0 < \phi_p < 1$, yield the volume fractions of PEO in phases at equilibrium. The phase separation curves of Figure 2 were obtained by plotting these points at different temperatures, for two different chain lengths. The curves show fairly good agreement with the experimental data. We use eq 6 with the coefficients expressed in Table 1 for further analysis.

## 3. Model for Adsorption of PEO on Solid Surfaces

The continuum model[23] is used here to describe the equilibrium thermodynamics of the system at the solid−liquid interface. We consider here a plane solid surface in contact with an infinite quantity of the solution consisting of a monodisperse polymer (PEO in this case) and a monomeric solvent (water). The space is divided into three regions, the bulk, the interphase, and the surface phase. The concentration of the polymer is uniform in the bulk. The interphase extends from $z = 0$ to $z = d$, $z$ being the distance measured normal to the surface with $z = 0$ representing the surface. In the interphase, the polymer concentration is only a function of $z$, the distance normal to the surface. The thickness of the interphase $d$ is chosen sufficiently large to ensure that the concentration gradients are negligibly small beyond $z = d$. The surface phase is the two-dimensional plane region located at $z = *$. Although, the locations $z = 0$ and $z = *$ are the same, polymer (or solvent) at $z = 0$ is not attached to the surface, while that at $z = *$ is. The molecules of the solid itself are not included in the surface phase. The concentrations in the bulk and the interphase are described by volume fractions while those in the surface phase are described by area fractions. The connectivity of the polymer segments is described by the following equation:

$$l\frac{\partial G_p(z,q)}{\partial q} = \frac{l^2}{6}\frac{\partial^2 G_p(z,q)}{\partial z^2} + [1 - e^{u_p(z)/kT}]G_p(z,q) \quad (8)$$

where $G_p(z,q)$ is the probability of locating the end segment of a polymer subchain with contour length $q$ ($0 < q < rl$), at location $z$, relative to the bulk, i.e., $z = d$. The term $u_p$ represents the potential of the polymer segment. Equation 8 is solved subject to the following boundary conditions

$$G_p(z,0) = e^{-u_p/kT} \quad (9)$$

$$G_p(d,q) = 1 \quad (10)$$

$$l\frac{\partial G_p(0,q)}{\partial q} = \left(1 + 2e\frac{(u_p(0) - u_p^*)}{kT}\right)^{-1}\left[\frac{l}{2}\frac{\partial G_p(z,q)}{\partial z}\Big|_{z=0} + G_p(0,q)\left\{1 - 2e\frac{u_p(0)}{kT} + 2e\frac{(u_p(0) - u_p^*)}{kT}\right\}\right] \quad (11)$$

Equation 9 states that the probability weight of the end of a subchain of zero contour length is entirely governed by its potential, since this end is free from any polymer attachment. Equation 10 is reminder of the fact that probability $G_p$ is weighted with respect to the bulk ($z = d$). Equation 11 is the boundary condition at $z = 0$ and is derived[23] by taking into account the spatial constraint imposed by the solid surface. The quantity $u_p^*$ in this equation represents potential acting on a polymer segment in the surface (*) phase. The potential $u_p(0)$ is different from $u_p^*$, since the later include the energetic interactions with the molecules of the surface. The probability $G_p^*(q)$ of finding the end of a subchain of length $q$ in the surface phase can be related to its

probability at $z = 0$ (in the unattached state) as

$$\frac{G^*_p(q)}{G_p(0,q)} = e^{-[u^*_p - u_p(0)]/kT} \tag{12}$$

The volume fraction of the polymer at location $z$ in the interphase is related to bulk volume fraction by the following equation:

$$\phi_p(z) = \frac{\phi^b_p}{rl} e^{u_p(z)/kT} \int_0^{rl} G_p(z,q) G_p(z, rl - q)\, dq \tag{13}$$

The area fraction of the polymer in the surface phase is given by

$$\varphi^*_p = \frac{\phi^b_p}{rl} e^{u^*_p/kT} \int_0^{rl} G^*_p(q) G^*_p(rl - q)\, dq \tag{14}$$

To determine the potential field in the interfacial region, we use the heuristic formalism developed by Evans and Needham. The total Helmholtz free energy of the system, consisting of the bulk phase, the interphase, and the surface phase can be written as

$$F = V^b \sum_k \frac{\phi^b_k}{v_k} \mu^b_k + V^b \xi^b \left(\sum_k \phi^b_k - 1\right) + A_s \int_0^d \sum_k \frac{\phi_k}{v_k} (\mu^h_k - \epsilon_k) + \zeta \left(\sum_k \phi_k - 1\right) dz + A_s \sum_k \frac{\varphi^*_k}{a_k} (\mu^{*h}_k - \epsilon^*_k) + A_s \zeta^* \left(\sum_k \varphi^*_k - 1\right) + \tau A_s \left( \int_0^d \frac{\phi_p - \phi^f_p}{v_p} dz + \frac{\varphi^*_p}{a_p} - \Gamma \right) \tag{15}$$

The summation index $k$ refers to the components of the solution, viz. the polymer (p) and the solvent (w). The space filling constraints that the volume/area fractions add to one in the three regions are introduced through the coefficients of the Lagrange multipliers $\xi^b$, $\zeta$, and $\zeta^*$. The terms $\epsilon_k$ and $\epsilon^*_k$ are the nonhomogeneous components of to the chemical potential in the interphase and the surface phase, respectively. Since the solvent is monomeric, its nonhomogeneous component is zero.

The last term is introduced to account for the situation, where the adsorbed amount of the polymer, given by the following expression

$$\Gamma = \int_0^d \left( \frac{\phi_p(z) - \phi^f_p(z)}{v_p} \right) dz + \frac{\varphi^*_p}{a_p} \tag{16}$$

is constrained at a value which is different from the equilibrium adsorbed amount ($\phi^f_p(z)$ in eq 16 is the volume fraction profile of the polymer which is not attached to the surface). Such a constraint occurs in a situation where, for example, the polymer is entrapped between two surfaces and is not allowed to escape or when the contact time of the solid with the fluid is not sufficiently long to allow the polymer to attain the equilibrium. The Lagrange multiplier $\tau$ is introduced in order to accommodate this constraint. For the equilibrium adsorption, this constraint is absent.

The free energy expressed in eq 15 is minimized with respect to the six variables, $\phi^b_k$, $\phi_k(z)$ and $\varphi^*_k$ ($k$ = p, w)-using the following constraints.

(i) The Gibbs−Duhem equations for the three regions:

$$\sum_k \frac{\phi^b_k}{v_k} \delta\mu^b_k = 0, \quad \sum_k \frac{\phi_k}{v_k} (\delta\mu^h_k - \delta\epsilon_k) = 0, \quad \sum_k \frac{\varphi^*_k}{a_k} (\delta\mu^{*h}_k - \delta\epsilon^*_k) = 0 \tag{17}$$

(ii) Constancy of total volume:

$$\delta V^b + A_s \delta d = 0 \tag{18}$$

(iii) Constancy of the total number of molecules of each species

$$V^b \frac{\delta\phi^b_k}{v_k} + \frac{\phi^b_k}{v_k} \delta V^b + A_s \int_0^d \frac{\delta\phi_k}{v_k} dz + A_s \frac{\phi^b_k}{v_k} \delta d + A_s \frac{\delta\varphi^*_k}{a_k} = 0 \tag{19}$$

The minimization of free energy and the subsequent simplification yield the following equations:

$$\mu^h_w(z) = \mu^b_w + v_w(\xi^b - \zeta(z)) \tag{20}$$

$$\mu^{*h}_w = \mu^b_w + a_w \left( \frac{v_w}{a_w} \xi^b - \zeta^* \right) \tag{21}$$

$$\epsilon_p = \mu^h_p - \mu^b_p - \frac{v_p}{v_w} (\mu^h_w - \mu^b_w) + \tau \tag{22}$$

$$\epsilon^*_p = \mu^{*h}_p - \mu^b_p - \frac{v_p}{v_w} (\mu^{*h}_w - \mu^b_w) + \tau \tag{23}$$

The term $\zeta(z)$ represents the tangential pressure at location $z$ in the interphase and $\zeta^*$ represents its analogue in the surface phase; $\xi^b$ represents the normal pressure, which is constant throughout the interfacial region. The difference $\xi^b - \zeta(z)$, therefore represents the contribution to the interfacial tension per unit height of the interface, whereas $v_w/a_w\xi^b - \zeta^*$ represents the contribution from the surface phase.

The expression for the free energy of the interfacial region, at equilibrium, can be obtained by substituting the expressions for $\epsilon_p$ and $\epsilon^*_p$ from eqs 22 and 23 respectively, into eq 15. Thus

$$F = V^b \left( \frac{\phi^b_p}{v_p} \mu^b_p + \frac{\phi^b_w}{v_w} \mu^b_w \right) + A_s \int_0^d \frac{\phi_p}{v_p} \left( \mu^b_p - \frac{v_p}{v_w} \mu^b_w \right) + \left( \frac{\mu_w}{v_w} \right) dz + A_s \left[ \frac{\varphi^*_p}{a_p} \left( \mu^b_p - \frac{a_p}{a_w} \mu^b_w \right) + \frac{\mu^*_w}{a_w} \right] - \tau A_s \left( \int_0^d \frac{\phi_p}{v_p} dz + \frac{\varphi^*_p}{a_p} \right) \tag{24}$$

The surface excess free energy can be obtained by subtracting, from eq 24, the free energy associated with same number of the molecules of the polymer and the solvent, but corresponding to the bulk composition. Thus, the excess free energy per unit area of the interface, $\gamma$, is

$$\gamma = \frac{F - F^b}{A_s} = \int_0^d \left( \frac{\mu^h_w - \mu^b_w}{v_w} \right) dz + \frac{\mu^{*h}_w - \mu^b_w}{a_w} - \tau\Gamma \tag{25}$$

The interfacial tension, $\gamma$, can also be written in an equivalent tangential pressure form as

$$\gamma = \int_0^d [\zeta^b - \zeta(z)]\, dz + \left[\frac{v_w \zeta^b}{a_w} - \zeta^*\right] - \tau\Gamma \quad (26)$$

where the term $\tau\Gamma$ represents the extra energy, per unit interfacial area, needed to retain $\Gamma$ amount of the polymer in the interfacial region.

The potentials of a PEO segment in the interphase and the surface phase are obtained by subtracting from the nonhomogeneous potentials (given by eq 22 and eq 23 respectively), the entropy associated with the polymer segment. The resulting expressions are

$$u_p(z) = (\mu_p^h(z) - \mu_p^b) - \frac{v_p}{v_w}(\mu_w^h(z) - \mu_w^b) - \frac{kT}{r}\ln\left(\frac{\phi_p(z)}{\phi_p^b}\right) + \tau \quad (27)$$

and

$$u_p^* = (\mu_p^{*h} - \mu_p^b) - \frac{a_p}{a_w}(\mu_w^{*h} - \mu_w^b) - \frac{kT}{r}\ln\left(\frac{\varphi_p^*}{\phi_p^b}\right) + \tau \quad (28)$$

Substituting the expressions for $\mu_w^h$ and $\mu_p^h$ from eqs 2 and 3, respectively, into eq 27, we obtain

$$\frac{u_p}{kT} = \frac{v_p}{v_w}\left[\chi(\phi_w - \phi_p) - \chi^b(\phi_w^b - \phi_p^b) + \phi_w\phi_p\frac{\partial\chi}{\partial\phi_p} - \phi_w^b\phi_p^b\frac{\partial\chi}{\partial\phi_p^b} - \ln\left(\frac{\phi_w}{\phi_w^b}\right)\right] + \frac{\tau}{kT} \quad (29)$$

where $\chi^b$ is the $\chi$ parameter corresponding to the bulk solution composition.

In the surface phase, which is a two-dimensional continuum, $\mu_w^*$ and $\mu_p^{*h}$ can be derived from eqs 2 and 3, respectively, by replacing volumes by areas and volume fractions by area fractions. In addition, we also introduce two additional terms $\chi_w^*$ and $\chi_p^*$, which are the energies of interaction, scaled by $kT$, of the solvent and the polymer with the solid surface, respectively. Thus

$$\frac{\mu_w^{*h}}{kT} = \ln(\varphi_w^*) + \varphi_p^*\left(1 - \frac{a_w}{ra_p}\right) + \chi'\varphi_{*p}{}^2 - \varphi_w^*\varphi_p^{*2}\frac{\partial\chi'}{\partial\varphi_p^*} + \chi_w^* \quad (30)$$

and

$$\frac{\mu_p^{*h}}{kT} = \frac{1}{r}\ln(\varphi_p^*) + \varphi_w^*\left(\frac{1}{r} - \frac{a_p}{a_w}\right) + \chi'\frac{a_p}{a_w}\varphi_w^{*2} + \varphi_w^{*2}\varphi_p^*\left(\frac{a_p}{a_w}\right)\frac{\partial\chi'}{\partial\varphi_p^*} + \frac{a_p}{a_w}\chi_p^* \quad (31)$$

In these equations, $\chi'$ is the two-dimensional analogue of the $\chi$ parameter and is, in general, a function of the area fraction of the polymer in the surface phase. We assume that the functional dependence of $\chi'$ on $\varphi_p^*$ and $T$ is the same as that of $\chi$ on $\phi_p$ and is given by eq 6.

Using eqs 30 and 31, we can rewrite eq 28 as

$$\frac{u_p^*}{kT} = \frac{v_p}{v_w}\left[\chi'(\varphi_w^* - \varphi_p^*) - \chi^b(\phi_w^b - \phi_p^b) + \varphi_w^*\varphi_p^*\frac{\partial\chi'}{\partial\varphi_p^*} - \phi_w^b\phi_p^b\frac{\partial\chi}{\partial\phi_p^b} - \ln\left(\frac{\varphi_w^*}{\phi_w^b}\right) - (\chi_w^* - \chi_p^*)\right] + \frac{\tau}{kT} \quad (32)$$

In this equation, we have assumed no density change accompanying the exchange of molecules between the solution and the surface phase. This requires that

$$\frac{a_p}{a_w} = \frac{v_p}{v_w} \quad (33)$$

We define the polymer−surface affinity parameter, $\chi^*$ as

$$\chi^* = \frac{a_p}{a_w}(\chi_w^* - \chi_p^*) \quad (34)$$

It represents the affinity of the polymer for the surface relative to the solvent.

The self-consistent field calculations begin with the initial guess of the volume fraction profile of the polymer in the interfacial region and also the area fraction of the polymer in the surface phase. The corresponding quantities for the solvent are obtained by noting that

$$\phi_w(z) + \phi_p(z) = 1 \text{ and } \varphi_w^* + \varphi_p^* = 1 \quad (35)$$

In the case of the equilibrium adsorption, $\tau = 0$, whereas for the adsorption under the constraint of a fixed adsorbed amount $\Gamma$, a suitable value of $\tau$ is assumed. The potentials of the polymer in the interfacial region and in the surface phase are then computed using eqs 29 and 32, respectively. Equation 8 is then solved in conjunction with the boundary conditions given by eqs 9−11, to obtain the probability weights $G_p(z,q)$ and $G_p^*(q)$. The volume fraction profile and the surface fraction are then obtained using eqs 13 and 14. For calculation of the adsorbed amount using eq 16, we need $\phi_p^f(z)$, the volume fraction profile of free (unattached) polymer. This is computed by resolving the connectivity equation but using the modified form of boundary condition 11, obtained by substituting $e^{-u_p^*/kT} = 0$ in the original equation. The volume and the area fractions are compared with the initial guesses of these quantities, and the new guessed values are generated. The computed adsorbed amount is compared with the guess value, and the difference is used for updating the value of $\tau$. The cycles of the calculations are repeated until the assumed and the computed values of $\phi_p(z)$, $\varphi_p^*$, and $\Gamma$ are very close. Once this task is accomplished, various characteristics of the adsorbed layer can be computed as discussed in section 4.

## 4. Determination of the Model Parameters

Various model parameters for PEO−water−silica system are obtained as follows.

**(i) Kuhn Length of PEO in Water.** Since the concentration of PEO solution in the major part of the interfacial region is in the semidilute or concentrated regime, the intramolecular excluded volume effect can be neglected. Hence the radius of gyration of PEO in the interfacial region would match the value at the Θ temperature and is reported as[32] $r_g^2 = d^2M_p$, with $d =$ 0.0343nm. Here, $M_p$ is the molecular weight of the polymer, noting that $r_g^2 = (1/6)rl^2$ and $M_p/M_m = rl/l_m$, where $l_m$ is the mean length of the backbone bonds of PEO monomer and is given by[33]

$$l_m = m\sqrt{[\sum_i^m l_i^2/m]} \tag{36}$$

and $M_m$ is the molecular weight of PEO monomer (=44). The sum in the eq 36 is taken over all the backbone bonds ($m$) in the monomer of PEO.

From these equations, we obtain the following expression for the Kuhn length of PEO.

$$l = \frac{6d^2M_m}{l_m} \tag{37}$$

PEO monomer has one C−C bond (length = 0.153 nm) and two C−O bonds (each of length = 0.143 nm). Hence $l_m = 3\sqrt{[(0.153)^2+2(0.143)^2]}/3 = 0.439$ nm. From eq 40, $l = 0.707$ nm. The number of segments $r$ in a PEO chain can now be obtained using the relation: $r = 0.0141M_p$.

**ii. Partial Volumes of the PEO Segment and Water.** The partial volumes of the PEO segment, $v_p$, and the water molecule, $v_w$, are obtained from the data on density of PEO solution,[26] as a function of the temperature. These data are in the range of PEO mass fractions 0.05−0.5, temperature range 278.15−333.15 K and for two molecular weights of PEO, viz. 6000 and 35 000. The solution density is practically independent of the molecular weight of the polymer. At a given temperature, the plot of molar volume ($v_m$) vs mole fraction of PEO is a straight line in the range of the mole fraction studied. The partial molar volumes of PEO and water are obtained from the intercepts of this plot on the $v_m$ axis at $x = 1$ and $x = 0$, respectively. These are linearly related to temperature. Thus

$$v_p = (6.880 \times 10^{-8}T + 38.60 \times 10^{-6})/N_{av}m^3 \tag{38}$$

and

$$v_w = (6.377 \times 10^{-9}T + 16.15 \times 10^{-6})/N_{av}m^3 \tag{39}$$

This yields the ratio of the partial molar volumes at 298 K as $(v_p/v_w) = 3.27$.

**iii. Partial Areas Occupied by PEO Segment and Water in the Surface Phase.** Values of the interfacial area occupied by polymer segment, $a_p$, needed for computing the amount of polymer in the surface phase, are estimated as follows. We first relate $a_w$ to $v_w$, by the following equation:

$$a_w = \left(\frac{3}{4}\right)^{2/3}\pi^{1/3}v_w^{2/3} \tag{40}$$

This assumes that the molecule of the solvent is a sphere, and its projection on the interface is a circle. We now obtain $a_p$ using eqs 33 and 40 as

$$a_p = \left(\frac{3}{4}\right)^{2/3}\pi^{1/3}v_w^{2/3}\left(\frac{v_p}{v_w}\right) \tag{41}$$

Substituting $v_p$ and $v_w$ from eqs 38 and 39, respectively, into eq 41, we can obtain $a_p$ as the function of temperature. The value of $a_p$ at 298 K estimated by this procedure is $3.819 \times 10^{-19}$ m$^2$·segment$^{-1}$.

**iv. The Polymer Surface Affinity Parameter $\chi^*$.** For the purpose of estimating $\chi^*$, we have used the experimental data of Trens and Denoyel[34] on enthalpy of displacement of water from silica by PEO. These experiments are conducted at 298 K and pH of 5.5, in a liquid flow microcalorimeter. In these experiments, a PEO solution is contacted with a plug of silica particles, of known surface area, which is preequilibrated with water. PEO displaces water from the silica surface. The amount of PEO adsorbing on the silica surface is controlled by varying both the feed PEO concentration and the time of contact of the fluid with the silica plug. The isothermal heat of adsorption and the amount of PEO adsorbed are measured. The plot of the heat of adsorption per mole of adsorbed monomer unit of PEO against the adsorbed amount is extrapolated to zero adsorbed amount. This limiting value is found to be −2.5 kJ·mol$^{-1}$. We make use of this information to determine $\chi^*$ as follows. In the limit of zero adsorption, eq 11 is simplified by substituting $G_p(0,q) = 1$, $u_p(0) = 0$, $\partial G_p(z,q)/\partial z|_{z=0} = 0$, and $\partial G_p(0,q)/\partial q = 0$. As a result of this we get

$$u_p^* = kT \ln 2 \tag{42}$$

This is the critical value of the surface potential at which no adsorption occurs.

We can also simplify eq 32, under this limiting condition, by substituting $\varphi_p^* = 0$ and $\varphi_w^* = 1$ into it, yielding

$$\frac{u_p^*}{kT} = \frac{a_p}{a_w}\left[\chi'\Big|_{\varphi^*_p=0} - \chi^b(\phi_w^b - \phi_p^b) - \phi_w^b\phi_p^b\frac{\partial\chi}{\partial\phi_p^b} - (\chi_w^* - \chi_p^*)\right] + \frac{\tau}{kT} \tag{43}$$

Since the bulk concentration of the polymer is very small, we can simplify the equation further to

$$\frac{u_p^*}{kT} = \frac{a_p}{a_w}[(\chi'|_{\varphi^*_p=0} - \chi^b) - (\chi_w^* - \chi_p^*)] + \frac{\tau}{kT} \tag{44}$$

Under this limiting condition of zero adsorption eq 25 can also be simplified as follows. Here, $\mu_w = \mu_w^b \approx 0$, and from eq 30, we have $\mu_w^{*h} = \chi_w^* kT$. Equation 25, therefore yields

$$\gamma = kT\frac{\chi_w^*}{a_w} - \tau\Gamma \tag{45}$$

Noting that $\gamma_w$, the free energy of adsorption of water

on the solid surface is given by

$$\gamma_w = kT\chi_w^*/a_w \tag{46}$$

we rewrite eq 45 as

$$\lim_{\Gamma\to 0}\left(\frac{\gamma_w - \gamma}{\Gamma}\right) = \tau \tag{47}$$

Combining eqs 42, 44, and 47, we obtain

$$\lim_{\Gamma\to 0}\left(\frac{\gamma - \gamma_w}{\Gamma}\right) = -kT\left[\chi^* - \frac{a_p}{a_w}(\chi'|\varphi_{p\to 0}^* - \chi^b) + \ln 2\right] \tag{48}$$

We note that the quantity on the left is the limiting heat of displacement per unit of the adsorbed PEO segment. If $\Delta H_m$ represents the heat of displacement per mole of PEO monomer, then it is related to the left-hand side of eq 48 as

$$\lim_{\Gamma\to 0}\left(\frac{\gamma - \gamma_w}{\Gamma}\right) = \frac{\Delta H_m l}{N_{av} l_m} \tag{49}$$

Combining eqs 48 and 49, and assuming, $\chi'|\varphi_{p\to 0}^* = \chi^b$, we obtain

$$\chi^* = \frac{(-\Delta H_m)l}{RTl_m} - \ln 2 \tag{50}$$

Using $\Delta H_m = -2.5$ kJ·mol$^{-1}$, we obtain: $\chi^* = 2500 \times 0.707/8.314 \times 298 \times 0.439 - \ln 2 = 0.93$.

We note from the above equation that the surface affinity parameter $\chi^*$ is lower than the measured enthalpy of displacement by an amount equal to ln 2. This additional exothermic heat appears as a compensation for the loss of the configurational entropy of the segment, when it is attached to the surface.

To test the accuracy of this surface affinity parameter, we have attempted to correlate the data of Trens and Denoyel on integral enthalpy of displacement of water by PEO, using our model. These data are obtained under the equilibrium conditions. Hence, we use $\tau = 0$. Combining eqs 25, 2, 30, and 46, we can derive the following expression for the integral heat of adsorption per unit interfacial area.

$$(-\Delta H_d) = \gamma_w - \gamma = -\frac{kT}{v_w}\int_0^d\left[\ln\left(\frac{\phi_w}{\phi_w^b}\right) + (\phi_p - \phi_p^b)\left(1 - \frac{v_w}{rv_p}\right) + \chi\phi_p{}^2 - \chi^b\phi_p^{b2} - \left(\phi_w\phi_p{}^2\frac{\partial\chi}{\partial\phi_p} - \phi_w^b\phi_p^{b2}\frac{\partial\chi^b}{\partial\phi_p^b}\right)\right]dz - \frac{kT}{a_w}\left[\ln\left(\frac{\varphi_w^*}{\phi_w^b}\right) + (\varphi_p^* - \phi_p^b)\left(1 - \frac{a_w}{ra_p}\right) + \chi'\varphi_p^{*2} - \chi\phi_p^{b2} - \left(\varphi_w^*\varphi_p^{*2}\frac{\partial\chi'}{\partial\varphi_p^*} - \phi_w^b\phi_p^{b2}\frac{\partial\chi^b}{\partial\phi_p^b}\right)\right] \tag{51}$$

Figure 3 presents the data on $(-\Delta H_d)$ vs molecular weight of PEO, $M_p$. The solid line represents the model prediction based on $\chi^* = 0.93$. From the plot, we find that the agreement at high molecular weights (>1000) is good. The deviation at lower molecular weight can be attributed to the end effect caused by the presence of the end OH groups. These OH groups form hydrogen bonds with the silanol groups on the silica surface. As a result, a significantly higher adsorption of the polymer results, yielding a higher value of $\Delta H$. To verify this, we estimate $\chi^*$ for PEG with molecular weight of 400, from the data of limiting enthalpy (obtained by the same authors), using eq 50, as 1.52. The integral enthalpy obtained using this value of $\chi^*$ is shown as a dotted curve. We note that this curve agrees fairly well with the experimental data of PEG 400.

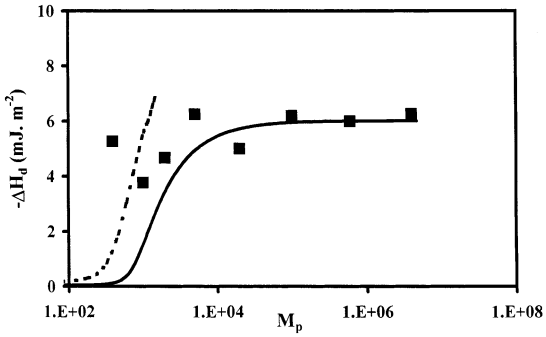


**Figure 3.** Heat of displacement of water from silica by PEO vs molecular weight of PEO at 25 °C. The experimental results are from Trens and Denoyal. The model fits are (—) with $\chi^* = 0.932$ and (···) with $\chi^* = 1.52$.

## 5. Results and Discussion

The aim of the present work is to compare the predictions of the model developed in the previous section, with the experimental data on adsorption of PEO from water on silica. Most of the authors report the data on surface excess of the polymer at the solid surface, which is defined as

$$\Gamma = \int_0^d\left(\frac{\phi_p(z) - \phi_p^b(z)}{v_p}\right)dz + \frac{\varphi_p^*}{a_p} \tag{52}$$

The surface excess is an ambiguous quantity since it decreases with increase in the bulk concentration of the polymer, beyond the concentration at which the adsorption plateau is reached. The adsorbed amount (defined by eq 16), on the other hand, remains constant beyond the plateau concentration and, therefore, is an unambiguous characteristic of the adsorbed layer. In the present work we have used adsorbed amount for comparison with the experimental data. This is justified on the basis of the fact that the surface excess differs very slightly from the adsorbed amount at the bulk concentrations not very far beyond the plateau concentrations, and these are the concentrations at which all the experiments are carried out.

**i. Adsorbed Amount in the form of Trains.** The adsorbed amount, Γ, can be divided into two parts. The train form (i.e., that lying in the surface phase), $\Gamma_{tr}$, and that in the form of loops and tails, $\Gamma_{lt}$. These quantities can be expressed in units of mg·m$^{-2}$ as

$$\Gamma_{tr} = \left(\frac{\varphi_p^*}{a_p N_{av}}\right)\left(\frac{M_m l}{l_m}\right) \times 10^3 \tag{53}$$

$$\Gamma_{ntr} = \left(\frac{\Gamma}{N_{av}}\right)\left(\frac{M_m l}{l_m}\right) \times 10^3 - \Gamma_{tr} \tag{54}$$

In Figure 4, we have compared the experimental data on the train amount for PEO−water−silica system,

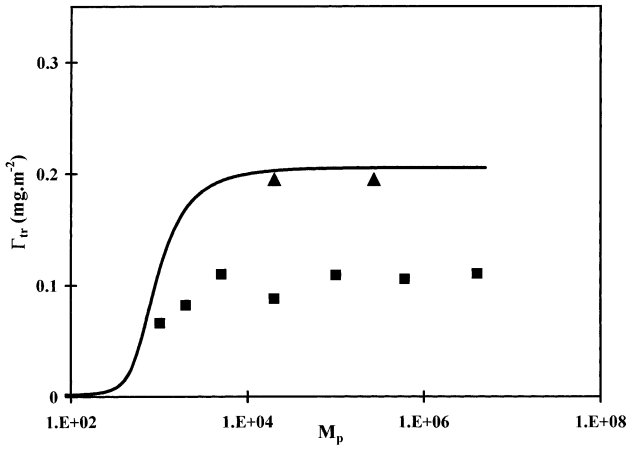


**Figure 4.** The amount of PEO in the form of trains on silica surface vs molecular weight of PEO at 298 K. The experimental data are from van der Beek et al.[35] (■), Trens and Denoyel[34] (▲). The solid curve represents model prediction.

obtained by two methods. The data of van der Beek et al.[35] have been obtained using proton NMR relaxation technique, whereas those of Trens and Denoyel[34] have been obtained using integral enthalpy of displacement (from Figure 3). The solid line represents the model prediction based on $\chi^* = 0.93$. A very good agreement between the model and the NMR data is seen. On the other hand, the data based on the enthalpy of displacement shows a very poor agreement. If we assume that the NMR data are correct, then it appears that the enthalpy data significantly underestimate the train amount. However, we emphasize here that this disparity is not caused by the enthalpy data in themselves (which are correct) but by the interpretation of these data. In the conventional procedure, used by Trens and Denoyel, the train amount is computed by dividing the enthalpy of displacement per unit area of surface by limiting value of the enthalpy of displacement per unit mass of the adsorbed polymer. This procedure ignores the effect of hydrogen bonding and also the entropy of adsorption. If these effects are ignored, the conventional analysis underestimates the train amount. That enthalpy data are consistent with the NMR data can be realized by the fact that our model agrees well both with NMR data (Figure 4) and with the enthalpy data (Figure 3). This brings out an important fact that both the enthalpy and the NMR data predict the same values of the train amount. This finding dispels the common belief that enthalpy data are not suitable for measurement of train fraction since the heat of adsorption evolves very slowly and hence is always underestimated.[36]

**ii. Effect of pH on the Amount in the form of Trains.** The effect of pH on the train amount should allow us to obtain the relation between pH and $\chi^*$. Silica surface in water undergoes hydration, producing silanol (SiOH) groups. The hydrogen of silanol group forms hydrogen bond with PEO−oxygen, and this bond is responsible for adsorption of PEO on silica. The strength of the hydrogen bond should depend on the surface density of silanol groups. With an increase in pH, silanol groups ionize. The resulting $SiO^-$ groups are unable to form a hydrogen bond with PEO oxygen. This results in an increase in $\chi_p^*$, the adsorption energy of polymer on silica. Moreover, $SiO^-$ can still form hydrogen bond with hydrogen atom of water. This means that $\chi_w^*$, the adsorption energy of water, does not increase to the same extent as $\chi_p^*$. Thus, $\chi^*$ [$= a_p/a_w(\chi_w^* - \chi_p^*)$] should decrease with increase in the pH of the solution. Consequently, the amount of PEO in the train form should also decrease. This is seen from Figure 5, in which we have plotted the data of van der Beek et al.[35] These data can be correlated as shown below.

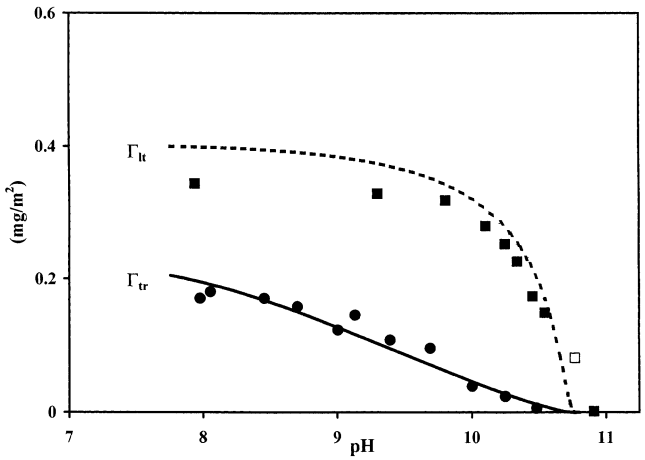


**Figure 5.** Effect of pH on adsorption of PEO on Silica (298 K, $M_p = 2.7 \times 10^5$). Experimental data points are from van der Beek et al.[35] (●) Represents the train amount. (■) Represents loop-tail amount. Solid curve (—) represents the theoretical predictions of the train amount and (- - -) that of the loop-tail amount.

Schindler et al.[37] have obtained the surface density of the ionized silanol groups by pH titration of activated silica, Aerosil 200, of known surface area. They have obtained the following relationship between pH and the surface density of the ionized silanol groups [$SiO^-$], expressed in number per square nanometers of the surface area.

$$\log [SiO^-] = 5.2 \log pH - 4.78 \qquad (55)$$

Let [Si] represent the surface density (nm$^{-2}$) of the silanol groups (sum of the dissociated and undissociated forms). Let the free energy of adsorption of a PEO on area of magnitude $a_w$ of the surface, totally in the form of silanol groups, be denoted by $-e_p$, and let the corresponding free energy of water be $-e_{w_1}$. Let us denote the free energy of adsorption of water per area $a_w$, in the form of fully ionized silanol groups by $-e_{w_2}$. All these are expressed in the units of $kT$. We can now write

$$\chi_p^* = -e_p\left(\frac{[Si] - [SiO^-]}{[Si]}\right) \qquad (56)$$

and

$$\chi_w^* = -e_{w_1}\left(\frac{[Si] - [SiO^-]}{[Si]}\right) - e_{w_2}\left(\frac{[SiO^-]}{[Si]}\right) \qquad (57)$$

Combining the above two equations with eq 34, we obtain

$$\chi^* = \frac{a_p}{a_w}\left\{(e_p - e_{w_1}) - (e_p - e_{w_1} + e_{w_2})\frac{[SiO^-]}{[Si]}\right\} \qquad (58)$$

From eq 58, it is clear that the plot of $\chi^*$ vs the fraction of the dissociated silanol groups should be a straight

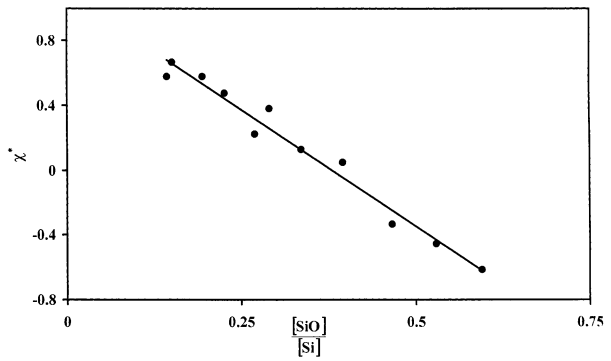


**Figure 6.** Adsorption energy parameter vs the extent of ionization of silanol groups. The solid line represents the linear regression fit. Data are computed from the experimental values of the train amount presented in Figure 5 using procedure described in the text.

line with slope $-a_p/a_w(e_p - e_{w_1} + e_{w_2})$ and the intercept on the $x$-axis as $a_p/a_w(e_p - e_{w_1})$.

To verify eq 58, we use the experimental data of Figure 5. For each of the experimental value of the train amount, we have back-calculated the value of $\chi^*$, using our model. Using the corresponding value of pH in eq 55, we have obtained the value [$SiO^-$]. The value of [Si], the total surface density of silanol groups, has been reported as 5.5−5.8 $nm^{-2}$.[37] We use the mean value of 5.65. Figure 6 shows a plot of $\chi^*$ vs [$SiO^-$]/[Si]. It is a straight line as expected on the basis of eq 58. The slope of the plot is −2.88 and the intercept on the $x$-axis is 1.10. Using the previously calculated value of $a_p/a_w$ = 3.27 the values of $(e_p - e_{w_1} + e_{w_2})$ and $(e_p - e_{w_1})$ are obtained as $0.88kT$ and $0.34kT$, respectively. This gives the value of $e_{w_2}$ as $0.54kT$. Taking the area $a_w$ as 0.025 $nm^2$, we can convert the above values to energies per silanol groups (per one hydrogen bond) and they read as $e_p - e_{w_1} = 2.4kT$ and $e_{w_2} = 3.8kT$. The value of $e_{w_2}$ lies in the typical range of the hydrogen bond energies ($1.7-4.8kT$).[38]

Combining eqs 55 and 58 and substituting the relevant values of the parameters, the following relation between $\chi^*$ and pH is obtained

$$\chi^* = 1.10 - 0.509\left(\frac{pH^{5.2}}{10^{4.78}}\right) \qquad (59)$$

The lower solid line in Figure 5 is the model prediction for the adsorbed amount in the form of trains, using the values of $\chi^*$ obtained from eq 59. The experimental values agree fairly well with the model prediction.

**iii. Adsorbed Amount in the form of Loops and Tails ($\Gamma_{lt}$).** Figure 7 shows the experimental data of various workers on the variation of $\Gamma_{lt}$ with the molecular weight of PEO. These data are obtained by subtracting the adsorbed amount in the form of trains from the total adsorbed amount (which corresponds to the plateau value). The train amount is calculated using the present model. There are some differences in pH of the solution used by these workers. All the experiments, however, fall in the pH range from 2.3 to 7.5. In this range of pH, $\chi^*$ varies from 0.8 to 1.1 according to eq 59. In this range, the loop tail amount is practically independent of $\chi^*$ and a single curve represents the model prediction. The deviation of the model from the experimental data is 21.3%, which is fair, considering the scatter in the experimental data.

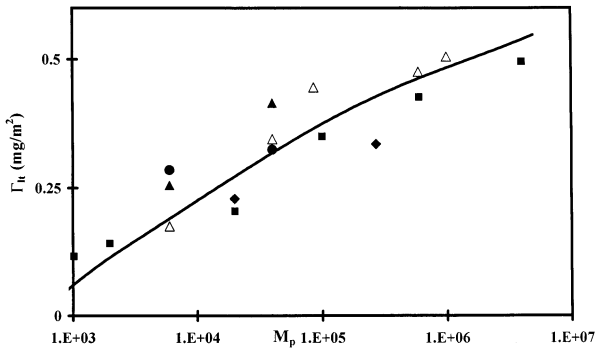


**Figure 7.** Variation of the amount of PEO in loops and tails on silica from aqueous solution at 298 K vs molecular weight. The experimental data are from van der Beek[35] [pH 7.5, ◆], Trens and Denoyel[34] [pH 5.5, ■], and Kilmann et al.[39] [pH 5.5, ▲; pH 4.7, △; pH 2.3, ●]. The solid curve represents model prediction.

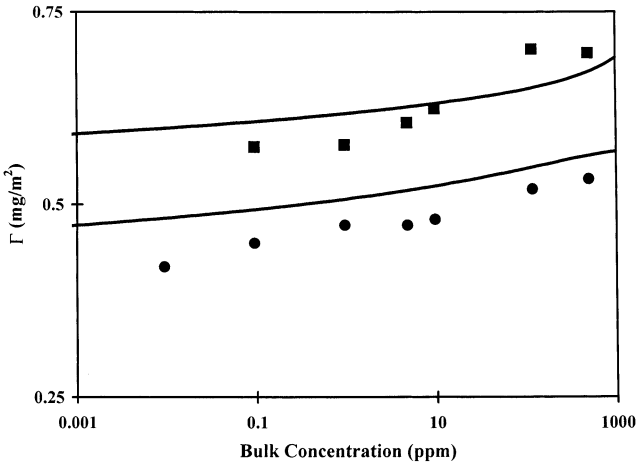


**Figure 8.** Adsorption isotherm of PEO at 25 °C: (■) $M_p$ = 963 000 (●) $M_p$ 120 000. The solid lines are the model predictions.

The effect of the bulk concentration of PEO on the adsorbed amount, at a constant chain length, obtained from the work of Fu and Santore,[40] is depicted in Figure 8. The solid lines are the prediction based on our model. The percent deviation of these data from the model prediction is 5.0% for PEO with $M_p$ = 963 000 and 9.0% for PEO with $M_p$ = 120 000.

The effect of pH on $\Gamma_{lt}$ is depicted in Figure 5. The solid curve is based on the theory. The percent deviation of these data from the model prediction is 10.3%, excluding the point corresponding to pH = 10.8 (the point indicated by unfilled square).

**iv. Hydrodynamic Thickness.** Hydrodynamic layer thickness, $d_h$, is calculated using the modified form of the model developed by Cohen Stuart et al.[16] Here we consider flow between two flat parallel plates. The adsorbed layer on each plate is divided into two parts, the surface phase and the interphase. The surface phase is viewed as an equivalent polymer layer with uniform polymer volume fraction of $\phi_p(z)|_{z=0}$. Since the total volume of polymer in the surface phase is $\varphi_p^* v_p/a_p$, the equivalent thickness of the surface phase is

$$s = \frac{\varphi_p^* v_p}{a_p \phi_p(z)|_{z=0}} \qquad (60)$$

The thickness of the interphase is d and the volume fraction profile in this layer is that obtained using our

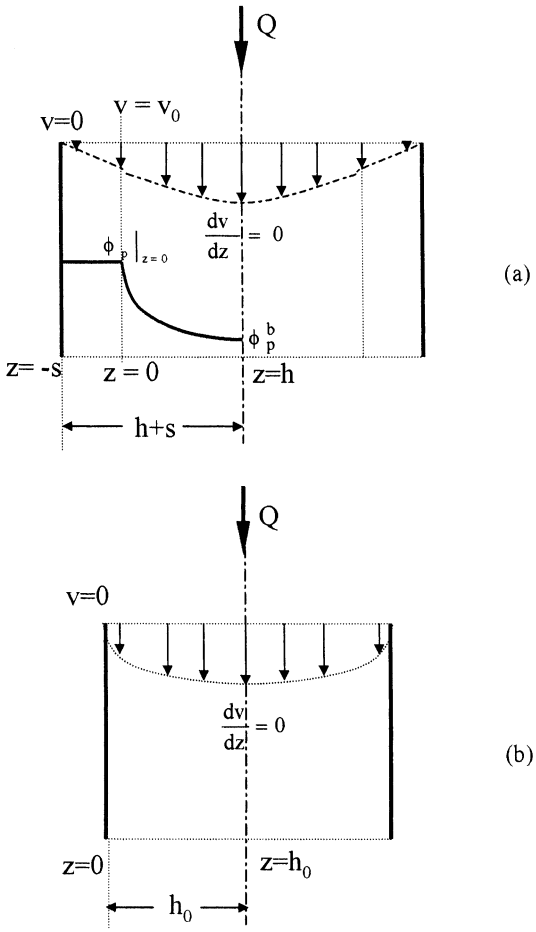


**Figure 9.** Model for hydrodynamic layer thickness: (a) two parallel plates with an adsorbed layer of polymer between them; (b) the parallel plates with no polymer. The distance between the plates are adjusted to yield the same $\Delta p$ in the two cases at a fixed value of $Q$.

model. We assume that the two plates are separated by the distance $2(h + s)$ as shown in Figure 9a. For calculation of the velocity profile in the interphase ($0 < z < h$), the Debye−Brinkman equation for laminar flow of Newtonian fluids through a porous medium is used.

$$\frac{d^2v(z)}{dz^2} - \frac{v(z)}{\kappa(z)} = \frac{(-\Delta P)}{\mu} \tag{61}$$

with the boundary conditions $v|_{z=0} = v_0$ and $dv/dz|_{z=h} = 0$. Here, $v(z)$ is the fluid velocity, $\mu$ is the viscosity of water, and $(-\Delta P)$ is the pressure drop per unit length of the plate. The term $\kappa(z)$ represents the permeability of the interphase and can be empirically related to the volume fraction profile by the following equation:

$$\kappa(z) = c\frac{1 - \phi(z)}{\phi(z)} \tag{62}$$

Here $c$ is a constant of proportionality and has an order of magnitude of 1 nm$^2$ as suggested by Mijnlieff,[41] based on his work on sedimentation, in both the good and the Θ solvents.

In the surface phase $-s < z < 0$, eq 61 reduces to

$$\frac{d^2v_s(z)}{dz^2} - \frac{v_s(z)}{\kappa} = \frac{(-\Delta P)}{\mu} \tag{63}$$

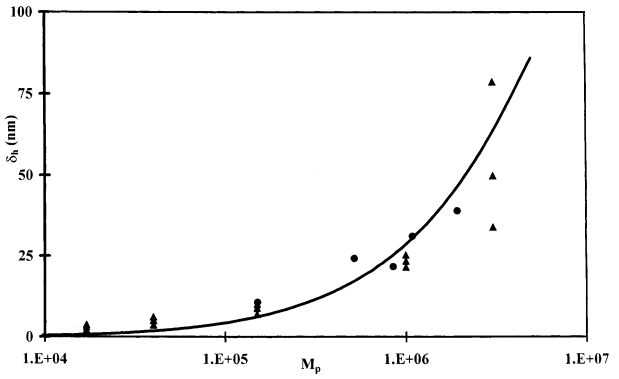


**Figure 10.** Variation of hydrodynamic thickness with molecular weight of PEO. Data points are ▲ (Killmann et al.[42]) and ● (Lafuma et al.[43]). Solid line represents the theoretical prediction.

with the boundary conditions $v_s|_{z=-s} = 0$ and $v_s|_{z=0} = v_0$.

In this region, the permeability of the adsorbed layer is considered to be constant, given by

$$\kappa = c\frac{1 - \phi(0)}{\phi(0)} \tag{64}$$

Equation 63 can be analytically solved to yield $v_0$ in terms of $(-\Delta P)$. Using this value of $v_0$, eq 61 is numerically solved in conjunction with eq 62, to obtain the velocity profile in the interphase in terms of $(-\Delta P)$. The total flow $Q$ through the gap between the plates is

$$Q = 2\int_{-s}^{h} v\, dz \tag{65}$$

In the absence of the polymer ($\kappa(z) \rightarrow \infty$), we can readjust the distance between the plates to a new value $2h_0$ (see Figure 9b) so that the volumetric flow rate $Q$ and $(-\Delta P)$ are the same as those in the presence of the adsorbed layer. The hydrodynamic thickness is then obtained as

$$d_h = h + s - h_0 \tag{66}$$

Figure 10 compares the experimental values of the hydrodynamic thickness of PEO layer on silica, obtained from several works,[42,43] with that computed using the model (solid curve). To fit these data the value of the constant $c$ used is 1.13 nm$^2$, which is very close to 1 nm$^2$ as suggested by Mijnlieff.[41] Again, the theory depicts the variation of hydrodynamic thickness with molecular weight of PEO very well.

In Figure 11, we have presented hydrodynamic thickness vs adsorbed amount. The experimental data are those reported by Killman et al.[39] Unlike other works, these experiments are conducted under nonequilibrium conditions. To compare the results with the theory, we have conducted simulations under the constraint of fixed adsorbed amount. The hydrodynamic thickness obtained is plotted as a solid line. Although the model predicts the experimental data at high-adsorbed amount very well, deviation at low-adsorbed amounts is significant. It is, however, important to note that, in this low range of the adsorbed amount, hydrodynamic thickness is very low (<6 nm) compared to the diameter of silica particles (100 nm), and factors such as surface roughness, particle shape, etc. can contribute significantly to the errors in the measurement of hydrodynamic radius.

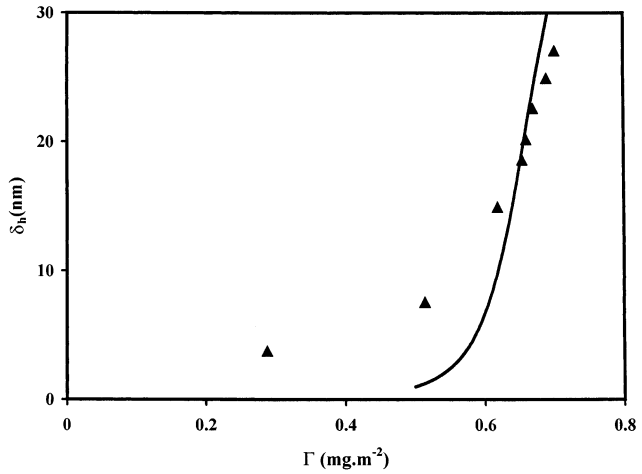


**Figure 11.** Hydrodynamic thickness vs adsorbed amount of PEO. Experimental results are from (▲) Killmann et al.[39] for PEO of $M_p$ 9.96 × $10^5$. Solid line represents the model prediction.

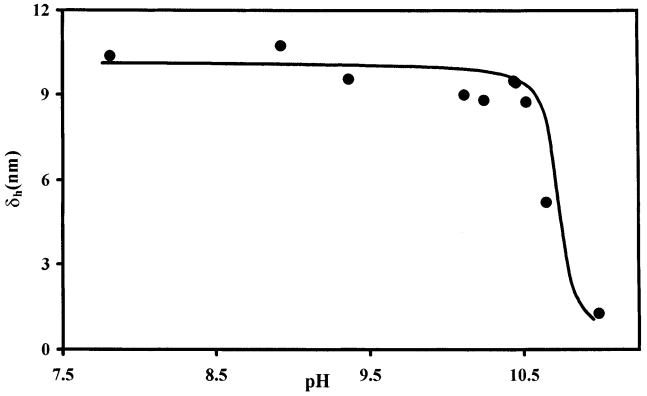


**Figure 12.** Variation of hydrodynamic thickness with pH. Experimental results are from van der Beek et al. for PEO $M_p$ 2.7 × $10^5$. Solid line is the theoretical prediction.

The effect of pH on the hydrodynamic thickness of adsorbed layer is presented in Figure 12. The solid line in this figure represents the model fit. The agreement between the experiment and the theory is good.

## 6. Conclusion

The analysis presented above indicates that it is possible to quantitatively predict the characteristics of the adsorbed layer by the continuum model for adsorption in conjunction with Evans−Needham model to obtain the self-consistent potentials of the polymeric species in the interfacial region. The hydrogen bond interactions can be accounted using any model, which expresses the free energy of a homogeneous polymer solution as a function of its composition. There is no need to modify the model to account for change in the hydrogen bond entropy due to anisotropy of the interfacial region. Although, for a binary system, the Flory−Huggins model with empirically fitted concentration-dependent $\chi$ parameter works well, as is shown here for the PEO−water system, for multicomponent systems, a more sound theoretical approach is needed for regression of the hydrogen bond parameters from the bulk solution activity data. These parameters can then be used for computing the homogeneous chemical potentials, $\mu_k^h(z)$, and subsequently, the self-consistent potential $u_p$, for the polymeric species.

Another important point brought out by this work is that calorimetry is a sound technique for measuring the contribution to the adsorbed amount from the trains. We have shown this through reconciliation of the calorimetric and NMR spin relaxation data on the PEO−water−silica system. The two techniques can complement each other in obtaining the idea of the extent of hydrogen bonding in the surface phase.

**Acknowledgment.** The authors would like to thank (i) Unilever Industries Private Limited for providing the funding for the research and (ii) Mr. V. M. Naik and Dr. S. J. Suresh from Unilever Research for valuable suggestions.

## Nomenclature

| | |
|---|---|
| $A_s$ | interfacial area, $m^2$ |
| $a_i$ | area occupied by a molecule of species $i$ in the surface phase, $m^2$ |
| $a_w$ | activity of water in aqueous PEO solution |
| $a(T)$, $b(T)$, $c(T)$ | constants defined in eq 6 |
| $c$ | permeability constants defined in eq 62 |
| $d$ | thickness of the interphase, m |
| $d_h$ | hydrodynamic layer thickness, m |
| $e_i$ | free energy of adsorption of species $i$ on the area $a_w$ of the silica surface, J |
| $F$ | free energy of mixing, J |
| $G_p(z,q)$ | probability weight for locating the end of a polymer subchain of length $q$ at location z |
| $G_p^*(q)$ | probability weight for finding the end of a polymer subchain of length $q$ in the surface phase |
| $h$, $h_0$ | distances between two parallel plates with and without polymer layer respectively, m |
| $\Delta H_m$ | specific enthalpy of displacement of water by PEO, $J \cdot mol^{-1}$ |
| $k$ | Boltzmann constant |
| $l$ | Kuhn length of polymer, m |
| $l_m$ | mean length of the backbone bonds of PEO monomer, m |
| $m$ | number of backbone bonds per monomer |
| $M_m$ | molecular weight of PEO monomer |
| $M_p$ | molecular weight of PEO |
| $N_{av}$ | Avogadro's number |
| $n_p$ | moles of PEO in the mixture |
| $n_w$ | moles of solvent (water) in the mixture |
| $-\Delta P$ | pressure drop, Pa |
| $Q$ | volumetric flow rate of water, $m^3 \cdot s^{-1}$ |
| $q$ | contour length of polymer chain, m |
| $r$ | number of segments in the polymer chain |
| $r_g$ | radius of gyration of the polymer chain, m |
| $s$ | equivalent thickness of the surface phase, m |
| $T$ | absolute temperature, K |
| $u_p$ | potential of the polymer segment, J |
| $V^b$ | volume of the bulk of the solution, $m^3$ |
| $v(z)$ | velocity profile of water, $m \cdot s^{-1}$ |
| $v_i$ | partial volumes of the polymer segment and water, respectively, $m^3$ |
| $v_m$ | molar volume of the solution, $m^3 \cdot mol^{-1}$ |
| $z$ | distance normal to the surface, m |

Greek Letters

| | |
|---|---|
| $\mu_i$ | chemical potential of the species $i$, $J \cdot mol^{-1}$ |

| | |
|---|---|
| $\chi$ | Flory−Huggins interaction parameter |
| $\phi_i$ | volume fraction of species *i* |
| $\varphi_i^*$ | area fraction species *i* in surface phase |
| $\Gamma$ | adsorbed amount of polymer, mg·m$^{-2}$ |
| $\zeta$ | Lagrange multiplier used for imposing the space-filling constraint |
| $\epsilon_i$ | inhomogeneity contribution to the chemical potential of species *i* |
| $\tau$ | Lagrange multiplier for imposing the constraint of fixed adsorbed amount |
| $\gamma$ | excess free energy per unit area of the interface, J·m$^{-2}$ |
| $\kappa$ | permeability of the adsorbed layer |
| $\mu$ | viscosity of the medium, Pa·s |
| $\beta_w$ | modified activity of water defined in eq 5 |

Subscripts

| | |
|---|---|
| p | polymer |
| w | solvent (water) |

Superscripts

| | |
|---|---|
| b | bulk value |
| f | free segment |
| $*$ | surface phase region located at $z = *$ |

## References and Notes


(1) Salamone, J. C. *Concise Polymeric Materials Encyclopedia*; CRC Press: New York, 1999.
(2) Avalson, F.; Panzer, H. P.; *Kirk Othmer Encyclopedia of Chemical Technology*, 3rd ed.; Wiley-Interscience: New York; 19XX; Vol. 10, p 489.
(3) Heitner, H. I.; Foster, T.; Panzer, H. P. *Encyclopedia of Polymer Science and Engineering*; Wiley-Interscience: New York; Vol. 9, p 824.
(4) Ryznar, J. W. U.S. Patent 3 492 224, 1970.
(5) Ghani, A. R.; Dunn, A. S. *Polym. Commun.* **1983**, *24*, 285.
(6) Fabini, M.; Bobula, S.; Rusina, M. *Polymer* **1994**, *35*, 2201.
(7) Levine, S.; Perram, J. W. In *Hydrogen Bonded Solvent Systems*; Covington, A. K., Jones, P., Eds.; Taylor and Francis: London, 1968.
(8) Veytsman, B. A. *J. Phys. Chem.* **1990**, *94*, 8499.
(9) Ikonomou, G. D.; Donohue, M. D. *Fluid Phase Equilib.* **1988**, *39*, 129.
(10) Panayiotou, C. G. *J. Phys. Chem.* **1988**, *92*, 2960.
(11) Panayiotou, C.; Sanchez, I. C. *J. Phys. Chem.* **1991**, *95*, 10090.
(12) Panayiotou, C.; Sanchez, I. C. *Macromolecules* **1991**, *24*, 6231.
(13) Cummings, P. T.; Stell, G. *Mol. Phys.* **1984**, *51*, 253.
(14) Wertheim, M. S. *J. Stat. Phys.* **1984**, *35*, 19; **1986**, *42*, 477.
(15) Segura, C. J.; Chapman, W. G.; Shukla, K. P. *Mol. Phys.* **1997**, *90*, 759.
(16) Cohen Stuart, M. A.; Waajen, F. H. W. H.; Cosgrove, T.; Vincent, B.; Crowley, T. L. *Macromolecules* **1984**, *17*, 1825.
(17) Scheutjens, J. M. M. H. M.; Fleer, G. J. *J. Phys. Chem.* **1979**, *83*, 1619; **1980**, *84*, 178.
(18) Suresh, S. J.; Naik, V. M. *J. Chem. Phys.* **1998**, *109*, 6021; *Langmuir* **1997**, *13*, 4785.
(19) Suresh, S. J.; Naik, V. M. *Langmuir* **1996**, *12*, 6151.
(20) Suresh, S. J.; Naik, V. M. *J. Chem. Phys.* **1999**, *111*, 10389.
(21) Evans, E. A.; Needham, D. *Macromolecules* **1988**, *21*, 1823.
(22) Ploehn, H. J. *Macromolecules* **1994**, *27*, 1627.
(23) Juvekar, V. A.; Anoop, C. V.; Pattanayek, S. K.; Naik, V. M. *Macromolecules* **1999**, *32*, 863.
(24) Quian, C.; Mumby, J. S.; Eichinger, B. E. *Macromolecules* **1991**, *24*, 1655.
(25) Bae, Y. C.; Shim, J. J.; Soane, D. S.; Praunitz, J. M. *J. Appl. Polym. Sci.* **1993**, *47*, 1193.
(26) Hasse, H.; Tintinger, K. R.; Maurer, G. *Macromolecules* **1995**, *28*, 3540.
(27) Haynes, C. A.; Beynon, R. A.; King, R. S.; Blanch, H. W.; Praunitz, J. M. *J. Phys. Chem.* **1989**, *93*, 5612.
(28) Herskowitz, M.; Gottlieb, M. *J. Chem. Eng. Data* **1984**, *29*, 173.
(29) Gaube, J.; Pfenning, A.; Stumpf, M. *J. Chem. Eng. Data* **1993**, *38*, 163.
(30) Saeki, S.; Kuwahara, N.; Nakata, M.; Kaneko, M. *Polymer* **1976**, *17*, 685.
(31) Bailey, F. E.; Callard, R. W. *J. Appl. Polym. Sci.* **1959**, *1*, 56.
(32) Fleer, G. J.; Cohen Stuart, M. A.; Scheutjens, J. M. H. M.; Cosgrove, T.; Vincent, B. *Polymers at Interfaces*; Chapman and Hall: London, 1993.
(33) Kawaguchi, S.; Imai, G.; Suzuki, J.; Miyahara, A.; Kitano, T.; Ito, K. *Polymer* **1997**, *38*, 2885.
(34) Trens, P.; Denoyel, R. *Langmuir* **1993**, *9*, 519.
(35) Van der Beek, G. P.; Cohen Stuart, M. A.; Cosgrove, T. *Langmuir* **1991**, *7*, 327.
(36) Cohen Stuart, M. A.; Fleer, G. J.; Bijsterbosch, B. H. *J. Colloid Interface Sci.* **1982**, *90*, 321.
(37) Schindler, P. W.; Furst, B.; Dick, R.; Wolf, P. *J. Colloid Interface Sci.* **1976**, *55*, 469.
(38) Perrin, C. L.; Nielson, J. B. *Annu. Rev. Phys. Chem.* **1997**, *48*, 511.
(39) Killmann, E.; Wild, T.; Gutling, N. *Colloids Surf.* **1986**, *18*, 241.
(40) Fu, Z.; Santore, M. M. *Colloid Surf., A: Phys. Chem. Eng. Aspects* **1998**, *135*, 63.
(41) Mijnlieff, P. F.; Wiegel, F. W. *J. Polym. Sci., Polym. Phys. Ed.* **1978**, *16*, 245.
(42) Killmann, E.; Maier, H.; Kaniut, P.; Gutling, N. *Colloids Surf.* **1985**, *15*, 261.
(43) Lafuma, F.; Wong, K.; Cabane, B. *J. Colloid Interface Sci.* **1991**, *143*, 9.


MA020478I